Exotic tree plantations in the Chilean Coastal Range: Balancing effects of discrete disturbances, connectivity and a persistent drought on catchment erosion

January 13, 2023

Abstract

The Coastal Range in the Mediterranean segment of the Chilean active margin is a soil mantled landscape able to store fresh water and potentially support a biodiverse native forest. In this landscape, human intervention has been increasing soil erosion for ∼200 yr, with the last ∼45 yr experiencing intensive management of exotic tree plantations. At the same time, this landscape has been affected by a prolonged megadrought, and how the anthropogenic disturbances and hydrometeorologic trends affect sediment transport is not yet well understood.

In this study we calculate a decadal-scale catchment erosion rate from suspended sediment loads and compare it with a 10^4-year-scale catchment denudation rate estimated from detritic ^{10}Be. We then contrast these rates against the effects of discrete disturbances and hydroclimatic trends. Erosion/denudation rates are similar on both time scales, i.e. 0.018 ±0.005 mm/yr and 0.024 ±0.004 mm/yr, respectively. Recent human-made disturbances include logging operations during each season and a dense network of forestry roads, which increase structural sediment connectivity. Other disturbances include the 2010 M_w 8.8 Maule earthquake, and two widespread wildfires in 2015 and 2017.

A decrease in suspended sediment load is observed during the wet seasons for the period 1986-2018 coinciding with a decline in several hydroclimatic parameters. The low 10^4-year denudation rate agrees with a landscape dominated by slow soil creep. The low 10-year-scale erosion rate and the decrease in suspended sediments, however, conflicts with both the observed disturbances and increased structural (sediment) connectivity. These observations suggest that, either suspended sediment loads and, thus, catchment erosion, are underestimated, and/or that decennial sediment detachment and transport were smeared by decreasing rainfall and streamflow. Our findings indicate that human-made disturbances and hydrometeorologic trends may result in opposite, partially offsetting effects on recent sediment transport, but both contribute to the degradation of the landscape.

Introduction

Over 75% of Earth's ice-free land has been altered by humans (Ellis and Ramankutty, 2008), with severe consequences for sediment transport during the Anthropocene (Syvitski et al., 2022). Land Use and Land Cover Changes (LULCC) are important in increasing soil erosion (Borrelli et al., 2020). Human-made forests – or better, tree plantations (DellaSala, 2020) – are frequently disturbed by logging and the implementation of forestry roads. Such disturbances may intensify soil erosion (e.g., Schuller et al., 2013; Sidle and Ziegler, 2012), as may heavy machinery traffic (e.g., Malmer and Grip, 1990), wildfires and terracing (e.g., Martins et al., 2013). Short rotational cycles, i.e. the period between planting, harvesting, and replanting of tree plantations, also change hillslope stability by cycles of root strength decay and recovery, which in turn promote landsliding and debris flows (Imaizumi et al., 2008; Montgomery et al., 2000). Ultimately, all such processes may modify sediment trajectories and storage on hillslopes and along rivers (Wainwright et al., 2011) with long-lasting impacts on sediment yields for periods of 10-100 years (Moody and Martin, 2009; Bladon et al., 2014).

The Chilean Coastal Range (CCR) in its Mediterranean section (35-37.5º S) is a landscape of gentle and largely convex hillslopes. Here, forests, soils and water are closely coupled (Galleguillos et al., 2021). This morphology results from relatively slow denudation rates by soil creep on regolith-mantled landscapes

[45] (Roering et al., 2007), yet modified by the underlying bedrock (Gabet et al., 2021). Currently, the remnants
[46] of secondary native forest stand on soils as thick as 2 m (Soto et al., 2019), suggesting such minimum
[47] soil depths under undisturbed conditions. In the absence of snow storage, these soils form a major fresh
[48] water supply along the Mediterranean CCR, which many rural communities rely on. Thus, decision-making
[49] regarding land management is strategic for the resilience of these communities (e.g., Gimeno et al., 2022),
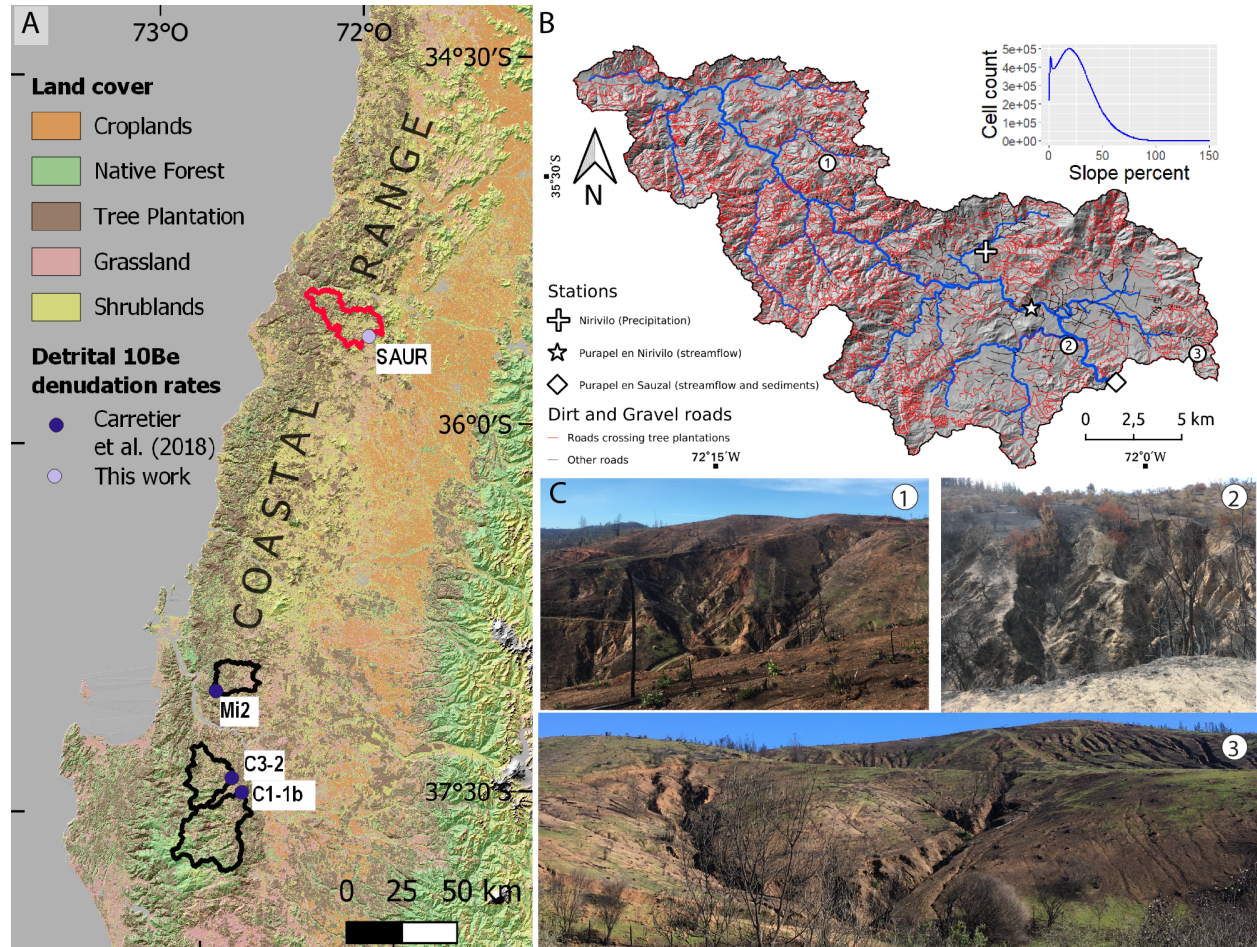[50] especially under recent (Garreaud et al., 2020) and projected (IPCC, 2021) conditions of water scarcity.

Figure 1: Study region. A. Land cover in the Coastal Range (Zhao et al., 2016) and catchments with published detrital [10]Be denudation rates outlined in black (Carretier et al., 2018). The Purapel catchment, which denudation rate is presented in this work, is represented in red. B. Purapel catchment. All the detected forestry roads intersecting tree plantations and the position of photos in C are shown. Elevation data comes from a 5-m resolution LiDAR DTM obtained in 2009. C. Photos captured on hillslopes of Purapel catchment.

[51] The CCR has experienced deforestation for more than 200 years (Armesto et al., 2010) intensifying soil
[52] erosion, as has been recognized by Bianchi-Gundian (1947) and Chilean governments in the middle of 20th
[53] century (IREN, 1965). From the beginning of 20th century, governments blamed environmental issues due to
[54] deforestation to promote the expansion of tree plantations (e.g., CONAF and MINAGRI, 2016; Pizarro et al.,
[55] 2020). The most relevant transformation of land cover began with the law DL 701 (1974) to subsidize the

Name	Denudat. rate (mm/yr)	Denudat. rate unc. (mm/yr)	Char. time (kyr)	Lat	Lon	Catch. area (km²)	Analyzed grain size (mm)	[¹⁰Be] (at/g)	[¹⁰Be] unc. (at/g)	Standard material	Source
SAUR	0.024	0.004	25	-35.6197	-72.0171	406	[0.5,1]	143751	5469	STD-11	This work
Mi2	0.037	0.006	16	-37.0488	-72.8614	235	[0.5,1]	93772	4280	4325	Carretier et al. (2018)
C3-2	0.039	0.007	15	-37.4052	-72.7976	357	[0.5,1]	97896	8272	4325	Carretier et al. (2018)
C1-1b	0.041	0.010	14	-37.4652	-72.7495	739	[0.5,1]	113680	20735	4325	Carretier et al. (2018)

Table 1: Published and new detrital ¹⁰Be denudation rates in the Mediterranean CCR. Denudation rates and their uncertainties were calculated with procedures described in Carretier et al. (2018). Characteristic time refers to the quartz residence time within a particle mean free path in rocks of 60 cm, and represent a timescale for steadily erosion (Lal, 1991). ¹⁰Be concentrations and their uncertainties were analyzed in the CEREGE laboratory with the indicated standard.

forestry sector (Manuschevich, 2020). This law and following political action accelerated LULCC, which in practice transformed degraded lands, shrublands and native forest into industrially managed tree plantations (Heilmayr et al., 2016). From ~450,000 ha of tree plantations in 1974 (Barros, 2018), their spatial extent increased to at least some 2.8 ±0.2 million ha in 2011 (Heilmayr et al., 2016), mostly within the Mediterranean CCR (Fig. 1).

In Chile, tree plantations are managed mostly as monocultures of fast-growing *Eucalyptus* spp or *Pinus Radiata*. The rotation cycles are as short as 9-12 and 18-25 years, respectively (INFOR, 2004; Gerding, 1991). As a consequence, the CCR ranks among the highest worldwide in terms of combined forest loss and gain (Hansen et al., 2013). (Hansen et al., 2013) identified tree cover, forest loss and gain from Landsat imagery which in turn provide time-series of spectral metrics at each pixel. Clear-cut areas in Chilean tree plantations are generally detectable at the Landsat resolution scale because the clear-cuts usually expand over entire hillslopes (Fig. 2). Such practice is permitted by current Chilean law, as clear-cutting requires environmental impact assessments only for harvest areas >= 500 ha/yr or >= 1,000 ha/yr in Mediterranean and Temperate regions, respectively (*Artículo Primero, Título I, Artículo 3, m.1* at Chilean Law 19.300, 2013).

Tree plantations frequently are intersected by dense networks of logging roads. These roads are intended to facilitate access and use of heavy forest machinery, storage and transport of timber, as well as the subsequent (re-)plantation. Logged hillslopes, like logging roads, are important sediment sources during storms and after wet-season clear-cutting (Schuller et al., 2013, 2021; Aburto et al., 2020). For example, Aburto et al. (2020) reported highest post-harvest soil loss in a catchment sustaining a one-year-old plantation. Post-harvest erosion is mainly rainfall triggered (Aburto et al., 2020; Schuller et al., 2013) and after exceeding specific rainfall intensity thresholds (Mohr et al., 2013). The erosional work efficacy depends on the logging season, which is higher for wet season logging (Mohr et al., 2014). At the storm to yearly scale (10^{-4}-10^0 yr), roads are prime sources and routers of sediments in catchments covered by tree plantations (Schuller et al., 2013). This is not surprising, since they remain bare and prone to compaction by heavy machinery transit. These roads often intersect streams, which form bypasses to preferentially route sediment (Fig. 2), increasing the efficacy of mass transfer within a geomorphic system, or sediment connectivity (Wohl et al., 2019). In this case, road networks modify the pathways of runoff and sediments, and may also modify thresholds of rainfall to trigger sediment detachment and transport (for example, due to soil compaction), potentially affecting

the structural and functional components of sediment connectivity, as defined by Wainwright et al. (2011). This shift is also relevant to constraining off-site impacts of soil erosion (Boardman et al., 2019).

Despite the increase in structural connectivity, sediment mobilization depends mostly on specific thresholds of rainfall. For example, hydrologic connectivity to initiate runoff in recently logged areas required a threshold of 20 mm/hr in rainfall simulations on tree plantations near Nacimiento (Mohr et al., 2013). In the absence of long term records of rainfall intensities, hydro climatic trends on rainfall and streamflow are relevant to interpret catchment erosion. In Central Chile (30-39°S), rainfall decreased at ca. 4% per decade between 1960 and 2016 (Boisier et al., 2018b), culminating in an unprecedented megadrought starting 2010 (Garreaud et al., 2020).

While the erosional response of logging is largely indisputable, hydrologic responses to tree harvest are ambiguous. On the one hand, logging may increase streamflow discharge in general and peak flow in particular (Iroumé et al., 2006), logging may also decrease streamflow discharge due to enhanced groundwater recharge immediately after logging (Mohr, 2013). The distinct responses may most likely vary with tree species and age, harvest size, forestry treatment (thinning, clear cutting, replanting), riparian buffer width, and especially, with the moisture storage decrease under recent drought conditions, which exacerbated declines in runoff (Iroumé et al., 2021).

In addition to the mega-drought, recent increase in both magnitude and frequency in wildfire affects relatively more tree plantations compared to alternative land cover (Bowman et al., 2019). This is likely because fuel is more abundant under dense plantation cover that connect large continuous tracts of the landscape. Instead, native species are more patchy (Gómez-González et al., 2017, 2018).

While the observed disturbances affecting the vegetation cover predict high sediment yields in rivers (e.g., Reneau et al., 2007; Brown and Krygier, 1971), the long and persistent decline in rainfall (Méndez-Freire et al., 2022; Tolorza et al., 2019) together with the high water demands of tree plantations is expected to reduce sediment detachment and mobilization assuming fluvial transport-limited conditions. To evaluate the impacts of these opposite responses and their potential effects in land degradation, we explore the catchment scale erosion of the Purapel river (406 km^2 of drainage area). To this end, we combine two distinct temporal scales (10^4 and 10^{-1} yr), explore discrete disturbance events (2017 and 2015 wildfire, 2010 earthquake, wet-season logging), and calculate sediment connectivity associated with forestry roads.

Materials and methods

The Purapel catchment

The Purapel river drains the eastern flank of the CCR. The climate is Mediterranean type. Mean annual rainfall is 845 mm, and mean minimum and maximum air temperatures are 7.2 and 20.3°C, respectively, and the fluvial system is exclusively pluvial (Álvarez-Garreton et al., 2018). The catchment is 406 km^2 and dominated by metamorphic (47.5%) and granitic (44.3%) lithologies. Elevation ranges between 164 and 747 m a.s.l. Most hillslopes are gentle (hillslope gradients around 16%), largely convex, and incised by gullies that converted this landscape into badlands (Fig. 1). CIREN (2021) classified most of those hillslopes as severely affected by soil erosion. The dominant soil types are Inceptisols and Alfisols (Bonilla and Johnson, 2012). Soil properties are highly variable in space. Yet, soils under tree plantations are generally thinner and depleted in soil organic matter. Throughout the entire soil profile, the soil bulk densities of Eucalyptus
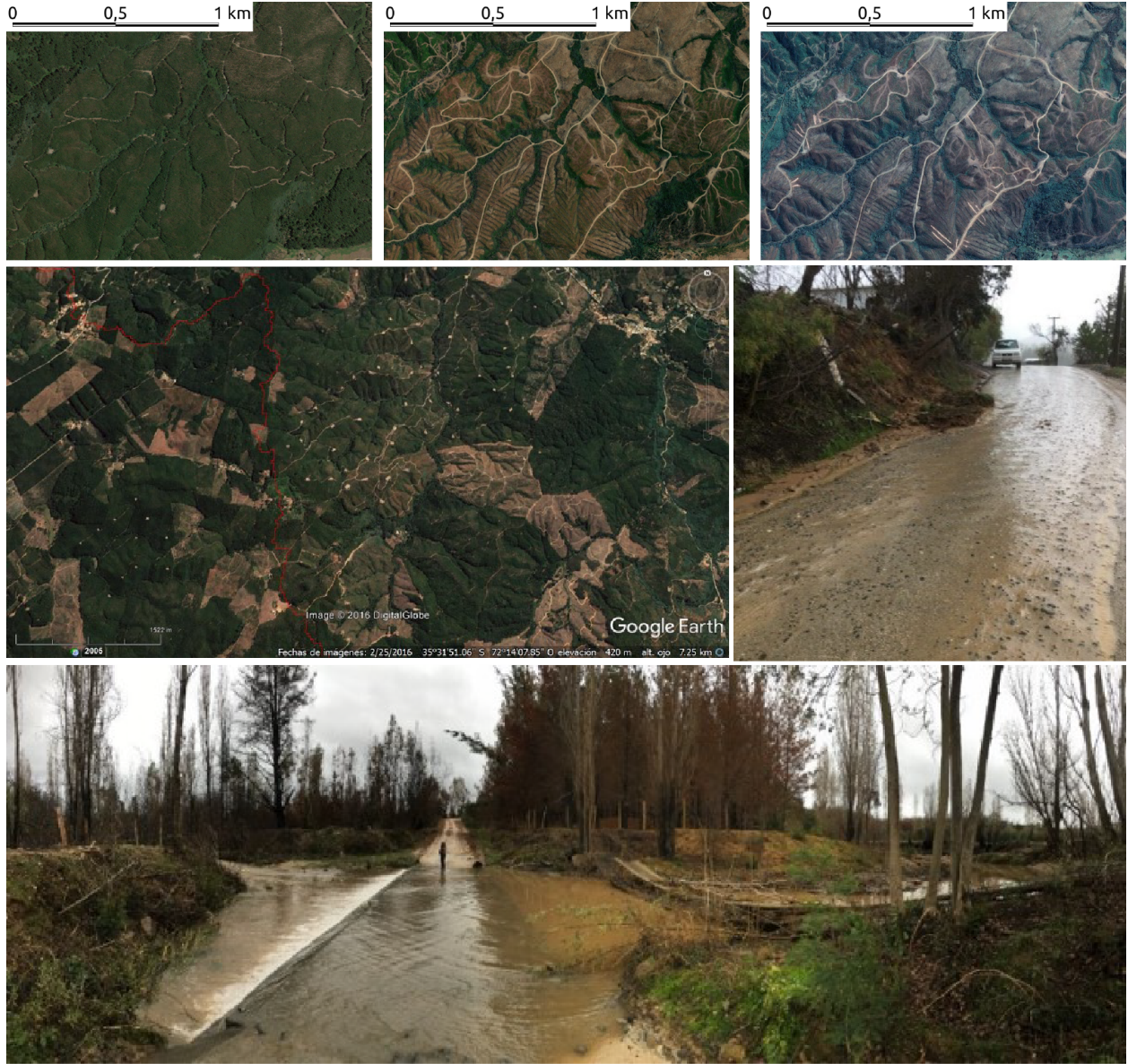
Figure 2: Details of forest roads in the Purapel catchment under different stages of the tree plantation rotational cycle and their connection to streams.

(1.38 ± 0.08 to 1.58 ± 0.12 g/cm^3) and Pine (1.28 ± 0.18 to 1.53 ± 0.13 g/cm^3) stands are higher than under native forests (0.89 ± 0.27 to 1.25 ± 0.24 g/cm^3) for depths between 0 to 60 cm (Soto et al., 2019).

Analysis of hydrometeorologic data

Due to the high spatio-temporal variability of rainfall, we tested local trends for available hydrometeorological data. To this end, we applied the Mann-Kendall test (Helsel et al., 2020) on time series of several hydrological variables. We also applied LOWESS smoothing (Cleveland, 1981) as a graphical expression of the main trends. We first evaluated the completeness of the data (supplementary material 1) and applied autocorrelation tests.

6

Rainfall, potential evapotranspiration and streamflow data from satellite and national stations are available in Mawüm (`https://mawun.cr2.cl/`) and CAMELS-CL (`https://camels.cr2.cl/`) sites. Suspended sediment data is available in the Chilean General Directorate of Water (DGA) site (`https://snia.mop.gob.cl/BNAConsultas/reportes`).

We analyzed annual and seasonal rainfall and potential evapotranspiration for several periods using both in situ (Nirivilo station) and gridded (CR2MET) data. The CR2MET product merges the ERA-Interim reanalysis, local topographic data, and the calibration with an updated national rain-gauge network (CR2MET, Boisier et al., 2018a). For annual data we excluded years with less than 330 data points and any month with less than 27 data points.

We also analyzed streamflow and suspended sediment loads to test for trends on annual, seasonal and monthly basis. The DGA estimated daily streamflows from single gauge stage readings using calibrated rating curves. Roughly once a month, the rating curves are updated by manual current meter measurements. The suspended sediment concentrations (SSC) were sampled on a daily-scale, too. All samples were obtained close to the water surface in vicinity of the water stage. The samples were filtered using a cotton linter cellulose paper with 80% of collection efficiency for particles larger than 0.3 μm (Advantec Qualitative Filter Papers 2, written communication from DGA operator). Then, they were dried, and combusted for 2 hours at 550-600°C in laboratories of the DGA (Solar, 1999).

The streamflow and SSC time series contain gaps. The gaps, however, are not seasonally clustered. Gaps during the dry season are mostly related to ceased streamflow (personal communication from DGA operator). We calculated daily suspended sediment discharge (t/day) as the product of streamflow discharge (m^3/s) and suspended sediment concentration SSC (mg/l), assuming those instantaneous measurements as representative of the entire day, thus converting seconds to day (Pepin et al., 2010). In addition, we calculated the number of data, the percentiles and the mean value of suspended sediment discharge for single hydrologic years, and the number of data and mean value of the three hydrometric parameters (streamflow, SSC and sediment discharge) from monthly to annual scales.

For annual streamflow and suspended sediments, we excluded the quantiles or averages for years with less than 185 data points and/or any month with less than 15 data points (around 50%). For seasonal streamflow and suspended sediments, we excluded seasons with less than 60 data points (around 66.6%). Here we define seasons as Summer (DJF), Autumn (MAM), Winter (JJA) and Spring (SON). We calculated the daily baseflow at Purapel en Sauzal station with the Lyne and Hollick filter (Ladson et al., 2013), which is a standard approach used in several studies (e.g. Li et al., 2022; Huang et al., 2021; Teutschbein et al., 2015; Zhang et al., 2017). We used several α values between 0.5 and 0.95 and $n.reflected$=30 days as parameters.

Catchment-wide erosion and denudation rates

We obtained catchment-wide erosion rates for Purapel river at the gauge "Río Purapel en Sauzal" using two approaches for different time scales, short-term (decadal) from suspended sediments and long-term (10^3 to 10^4 yrs) from detrital ^{10}Be. We calculated the long-term denudation rate to establish a benchmark to compare the recent sediment yields against. In most fluvial catchments the long-term rates exceed the short-term rates (Covault et al., 2013). This picture, however, may flip vice versa if soil erosion is high (Hewawasam et al., 2003; Vanacker et al., 2007). A limitation of our approach is the fact that detrital ^{10}Be rates include physical erosion and chemical weathering rates (von Blanckenburg and Willenbring, 2014),

while suspended sediment yields account only for physical erosion of very fine sediment (Summerfield and Hulton, 1994), which excludes bedload and dissolved load. Thus, we regard our short-term erosion rates as minimum rates for landscape lowering.

For the short-term, we calculated the mean specific sediment discharge (t/km^2/yr) as the average of all records (06/1985 to 11/2018) on a yearly scale and normalized by catchment area (Pepin et al., 2010). We estimated resulting erosion rate (mm/year) assuming a mean soil bulk density of 2.6 g/cm^3 (Carretier et al., 2018).

For the long-term, we assume the ^{10}Be concentrations within fluvial sands are proportional for catchment-wide averaged denudation rate (von Blanckenburg, 2005; Granger and Schaller, 2014). This rate integrates over a characteristic timescale that is inversely proportional to the denudation rate. These timescales are commonly longer than 10^3 years (Covault et al., 2013). We therefore regard the ^{10}Be derived rates as a reference that largely excludes recent human disturbances but includes low frequency and high magnitude erosion events (Kirchner et al., 2001). We obtained a bulk sample of fluvial sands from the active river bed along a cross section close to the water stage "Río Purapel en Sauzal". To this end, we use a standard sampling protocol, collecting sands from the surface at three locations within ∼10 m distance. We mixed all samples and sieved to a grain size fraction 0.5-1 mm. The mixed sand sample was processed at the French AMS ASTER facility in CEREGE (Standard STD-11).

Land cover changes

The Purapel catchment has experienced high rates of LULCC since the 19th century. This was largely due to the extensive increase in wheat production caused by the gold rushes in California and Australia (Cortés et al., 2022). Later on, between 1955 and 2014 tree plantations increased from (a minimum of) 10.27 (Hermosilla-Palma et al., 2021) to 203.5 km^2 (Zhao et al., 2016). Recently, two large wildfires burned the catchment: In 2015 14% of the catchment area burned. In 2017 almost the entire catchment burned (95%) (Tolorza et al., 2022).

To describe recent LULCC in this catchment, we use land cover maps both from compiled sources (1955, 1975 and 2017) and from our own (1986, 2000, 2005, 2010 and 2015):

- The 1955 and 1975 land cover maps of Hermosilla-Palma et al. (2021) cover the headwaters of the Purapel catchment (157 km^2). These maps were made interpreting the land cover from the 1:70,000 aerial photograph (Hycon flight) for 1955, and from the 60 m resolution Landsat-2 MMS and the 1:30,000 aerial photographs of 1978 (CH-30 flight) for 1975.

- We used Landsat Surface Reflectance products to identify land cover classes during dry seasons of 1986, 2000, 2005, 2010 and 2015. We classified unburned land cover using the Maximum Likelihood Classifier (Chuvieco, 2008) which we trained and validated with 20 and 10 polygons for each class, respectively. We validated the results with field observations during 2014-2015. We sub-classified burned surfaces into low, moderate and severe fire according to the differences in NBR index of pre- and post- fire images (thresholds <0.1 - 0.269>, <0.27 - 0.659>, <0.66 - 1.3> Key and Benson, 2006).

- The Land cover map of 2017 was made by Tolorza et al. (2022) with pre-fire Sentinel and LiDAR data. Here, this classification was resampled to 30 m resolution, to be compatible with LANDSAT classifications.

Logging roads and sediment connectivity

To identify changes in the structural connectivity we applied the Connectivity Index (IC, dimensionless) using the weighting factor (W, dimensionless) of (Cavalli et al., 2013). IC is a semi-quantitative approach to describe the degree of coupling between hillslopes and a target (for example, the stream network):

$$IC = \log_{10} \left(\frac{\overline{W}\,\overline{S}\sqrt{A}}{\sum\limits_i \dfrac{d_i}{W_i S_i}} \right) \tag{1}$$

, where $\overline{W}$ and $\overline{S}$(m/m) are the average weighting factor and slope gradients on the upslope contributing area (A, m^2), respectively. d_i (m), W_i (dimensionless) and S_i (m/m) are the path length, the weighting factor and the slope gradient on the ith cell in downslope towards a target.

W is calculated from a DTM to account for the effect of topographic roughness. The Roughness Index (RI, m) is the standard deviation of the residual topography. The residual topography refers to the difference between the original DTM and a smoothed version obtained by averaging DTM values on a 5×5 (=25) cell moving window:

$$RI = \sqrt{\frac{\sum\limits_i^{25}(x_i - x_m)^2}{25}} \tag{2}$$

, where x_i (m) is the value of one specific cell of the residual topography within the moving window, and x_m (m) is the mean of all 25 window cells. The weighting factor is calculated as:

$$W = 1 - \frac{RI}{RI_{max}} \tag{3}$$

, where RI_{max} is the maximum value of RI in the study area.

We quantified changes in sediment connectivity due to the forestry roads, RC, as

$$RC = IC_{rs} - IC_s \tag{4}$$

, where the subscripts s and rs refer to the stream network and and to the stream network including roads. We fed the model with a mapped forestry road network obtained from images available in the OpenLayers plugin of QGIS and post-2017-fire Sentinel compositions.

Disturbances in vegetation

We used the Breaks For Additive Season and Trend algorithm (BFAST, Verbesselt et al., 2010) on a LAND-SAT collection to detect disturbances in vegetation at the pixel scale, i.e. $>= 30$m. In the Purapel catchment, disturbances > 30 m are mostly due to wildfires and/or clear-cuts. Such disturbances lean on the seasonal behavior of the NDVI index on a time series of LANDSAT surface reflectance (Level 2, Collection 2, Tier 1) for the period from 09/1999 to 10/2021. Clouds were filtered using the QA band which uses the CFMask algorithm (Foga et al., 2017). We used the same parameter set as Cabezas and Fassnacht (2018), namely the threshold value for disturbances set to 93 manually labeled reference polygons with fire events, clear-cuts and constant tree-cover. It's worth mentioning, that we applied a sieve filter to the results. Hence, only

9

disturbances greater than 1 ha were considered. We trained the algorithm with the Landsat time series of 1999 to 2001. Given the disturbance regime of Purapel catchment (two large wildfires and possible loggings each 9 to 25 years) we run BFAST anticipating three possible breaks for the period 2002-2021. The accuracy assessment was performed on 35 manually drawn polygons that were randomly distributed across the catchment.

Results

Hydro climatic trends

At the annual scale at Nirivilo rainfall station, most data of the period 1962-2015 passed our completeness assessment criteria (53 of 54 years). In the case of CR2MET, the longest period analyzed here is 1979-2019. Judging from Mann-Kendall tests and LOWESS smoothing, we did not find a single trend for the longest interval of records (1962-2015). Nevertheless, for the period after 1979, we see decreasing non-monotonic trends for rainfall both at Nirivilo station and for CR2MET product. That decrease is steeper for 2000-2019, but less pronounced for intermediate intervals such as 1986-2018. During 1986-2018, however, a decrease in seasonal rainfall is observed for Autumn, at the beginning of the hydrologic year (Fig. 3). Generally, the Aridity Index (AI) follows similar decreasing trends as is the case for rainfall. For only 2 years (1982 and 2002) the AI was higher than 1. During all other years, potential evapotranspiration exceeded rainfall, thus indicating persistently dry conditions across this catchment.

Streamflow data is available at Purapel en Nirivilo between 1979 and 2019 and at Purapel en Sauzal between 1981-2019. At the annual scale, only 20 and 22, respectively, discontinuous years passed the completeness test. For Purapel en Sauzal streamflow data, results of baseflow separation are in the supplementary material 2. We selected the results obtained with $\alpha=0.7$ for further trend analysis, given the observed magnitudes and shape of the baseflow time series. For the Suspended Sediment Concentration data, the longest period is 1985-2018, but only 15 discontinuous years passed the completeness test. Because most of the annual time-series failed the autocorrelation and completeness tests, here we report only the seasonal analysis for Purapel en Sauzal station (Fig. 4). Although none of those time-series is monotonic, the sharp decrease in suspended sediment concentrations is clear for the three wetter seasons (Autumn, Winter and Spring).

Catchment-wide erosion and denudation rates

[10]Be denudation rater resulted in 0.024 $\pm$0.004 mm/yr (table 1), assuming a soil bulk density of 2.6 t/m^3. This rate translates into a sediment yield of 62.4 $\pm$ 10.4 tkm^{-2}yr^{-1}. This rate integrates over a characteristic timescale of $\sim$25 kyrs. Together with published data, detrital [10]Be denudation rates in the CCR point to between 0.02 and 0.05 mm/yr (table 1 Carretier et al., 2018), which are low compared to the global data for catchments of similar size (Covault et al., 2013).

Given the data completeness test we assume the decadal catchment-wide erosion rate from suspended sediments to be a conservative estimation. Following Pepin et al. (2010) we calculated the mean specific sediment discharge for all the records between 1985 and 2018 and a 30% of error (Pepin et al., 2010). For the Purapel catchment we estimate 46.99 $\pm$ 14.09 tkm^{-2}yr^{-1}, equal to 0.018 $\pm$0.005 mm/yr, assuming the same soil bulk density. Both rates do not statistically differ (Fig. 5).
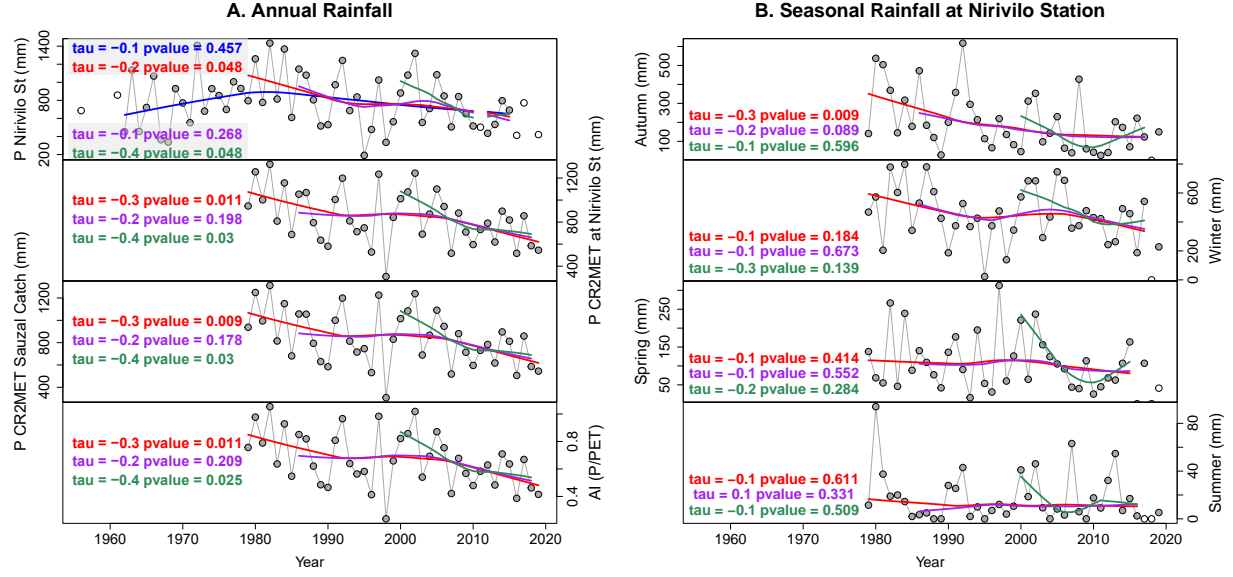
Figure 3: Annual and seasonal rainfall and annual aridity index (AI) at Purapel catchment. Main monotonic trends are tested with Mann-Kendall and LOWESS smoothing for 1962-2015 (blue), 1979-2019 (red), 1986-2018 (purple) and 2000-2018 (green). Unfilled circles are discarded data. A. Annual rainfall and AI time series. B. Seasonal time series for Nirivilo station.
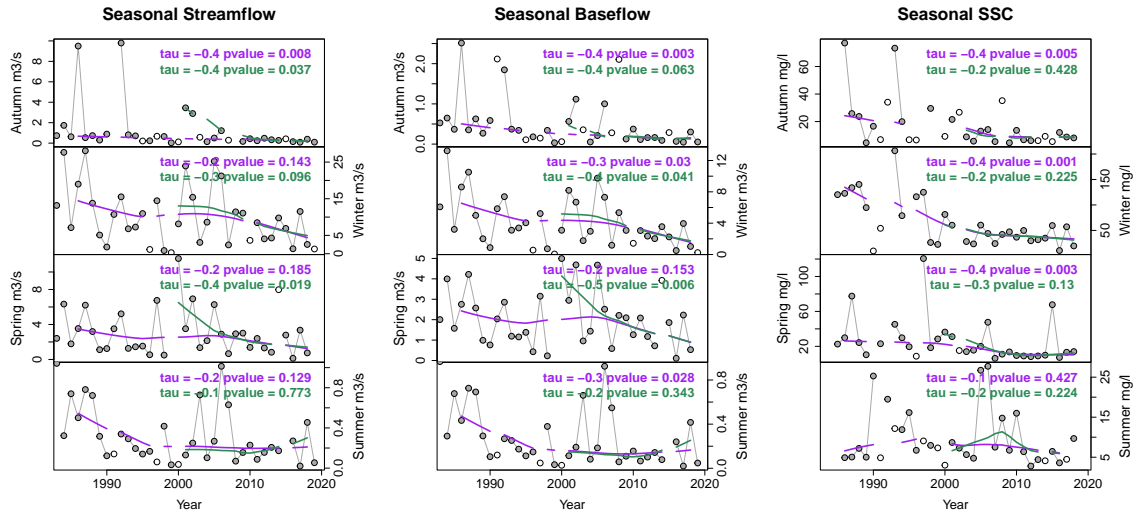

Figure 4: Mean seasonal streamflow, baseflow and suspended sediment concentrations at "Purapel en Sauzal" station. Main monotonic trends are tested with Mann-Kendall and LOWESS smoothing for 1986-2018 (purple) and 2000-2018 (green). Unfilled circles are discarded data. A. Streamflow at Purapel en Sauzal station. B. Baseflow at Purapel en Sauzal station. C. Suspended sediment concentrations at Purapel en Sauzal station.
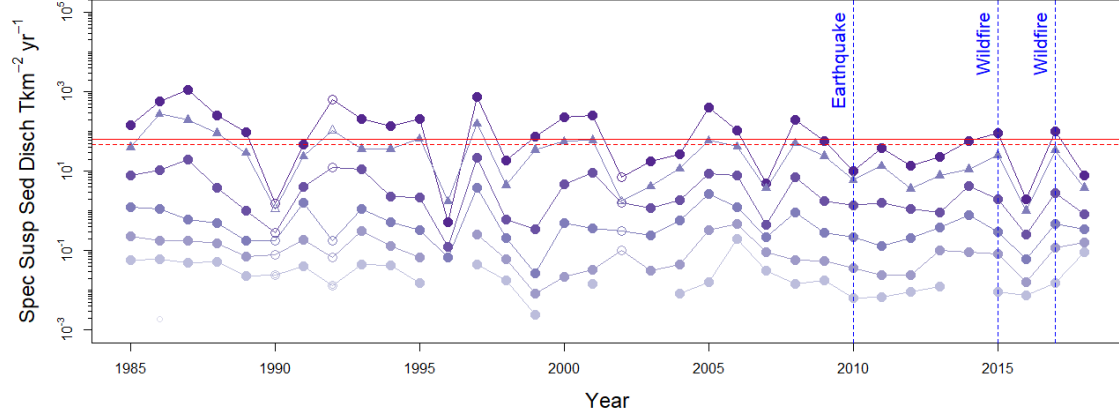
11

Figure 5: Denudation and specific suspended sediment discharge at Purapel en Sauzal gauge. Distributions of suspended sediment discharge for individual hydrologic years (March to Feb). Purple circles show percentiles (0.05, 0.25, 0.5, 0.75 and 0.95) and purple triangles show the mean. Filled symbols represent years with more than 185 daily data. Catchment erosion/denudation rates are indicated in red. Solid line is the sediment yield equivalent to the ^{10}Be denudation rate, dashed line is the average of all suspended sediment records.

Recent land cover changes

We developed five land cover maps for the period 1986-2015. The overall classification accuracy ranged between 83% and 92%. We distinguished between tree plantations, native forests, shrublands and seasonal grasslands. Seasonal grasslands included bare surfaces, seasonal pasture and sparse vegetation. We also classified seasonal grasslands to separate recently logged areas (clear-cuts) from other poorly vegetated areas.

Fig. 6 shows that the upper catchment was covered by a minimum of 1,000 ha of tree plantations and 5,500 ha of shrublands in 1955 (Hermosilla-Palma et al., 2021). Between the 1980s and the beginning of 21st century, the most prominent change comprised the transition from seasonal grasslands and shrublands into tree plantations. The first two classes covered a minimum of 23,550 ha in 1986 and 13,050 ha on 2005. During the same period, tree plantations expanded from 8,090 to 20,980 ha. Between the wildfires of 2015 and 2017, seasonal grasslands and shrublands together expanded to ∼20,300 ha (Fig. 6).

Landscape disturbances

The result of our mapped road network is illustrated in Fig. 1. Using this road network on a 5 m resolution LiDAR, we estimate some 18,000 ha of increased sediment connectivity, resulting in RC >0 (Fig. 7). RC values exceeding the 95-percentile (>3.12) are 1,986 ha. That surface of high RC is mostly located on hilltops: 1,966 ha (i.e. 99%) resulted in upstream contributing area <1 ha. Particularly these topographic settings exceed an empirical threshold between high and low connectivity for a mountain catchment, i.e. -2.32 (Martini et al., 2022). In the Purapel catchment the area above this threshold increased from 1,120 to as much as 6,570 ha simply due to the dense road network. This quantification, however, is done with a digital terrain model of coarser resolution compared to the original study of Martini et al. (2022) (5 m vs

12

0.5 to 2.5 m).

Based on our BFAST modeling, we obtained monthly time series of disturbances for 2002-2019 that we aggregate at the seasonal scale. We achieved a confusion matrix with a balanced accuracy of 0.86 and a F1 score of 0.69. For the complete period (Fig. 8A) 13,640 ha of the Purapel catchment (33.7%) experienced one break in the NDVI time series, 16,810 ha (41.5 %) showed two breaks and 5,010 ha (12%) presented three breaks. The undisturbed 12.8% included tree plantation stands that remained unlogged, and seasonal grasslands that remained poorly vegetated. Considering the seasonality (Fig. 8B), the 2015 and 2017 wildfires disturbed the catchment in the summer (dry season). Both wildfires were detected in ~5,000 and 24,000 ha, respectively. The disturbances that follow in area (~2,000 ha in 2002 and 1,910 ha in 2007) occurred during Autumn, corresponding to the first wet season of the hydrologic year. The largest surface disturbed during a Winter and a Spring were 770 ha each in 2006 and 2009, respectively.

Compared to the dNBR classification for 2017 (Tolorza et al., 2022), the BFAST results detected lower burned areas for the 2017 wildfire (33,618 vs 24,299 ha). This difference could be explained by the better capabilities of the dNBR index to detect burned areas, since it is a dedicated method to classify burned surfaces based in the NBR index of a pre- and a post- fire image (Key and Benson, 2006), while the BFAST algorithm was applied here on the NDVI, which is a index more suitable to detect the density of vegetation, and thus more sensitive to clear cuts.

Discussion

Both [10]Be denudation rate and suspended sediment erosion rate are surprisingly similar (Fig. 5). Hence, we argue that the suspended sediment samples capture at least the effects of erosion events recorded on the long-term. Both rates are low for fluvial catchments between 100-1,000 km^2 on a global scale (Covault et al., 2013). Yet, those rates are similar to 3 tributaries of the Biobío river draining the eastern CCR, which are between 0.037 ± 0.006 and 0.042 ± 0.008 mm/yr (Carretier et al., 2018). The low [10]Be denudation rate agrees with a landscape dominated by slow soil creep with occasional mass wasting triggered by earthquakes. There were only two reported landslides after the 2010 within the catchment area (Serey et al., 2019). Short term erosion does not exceed the long term denudation, as in other highly human-disturbed catchments (Hewawasam et al., 2003; Vanacker et al., 2007). Considering the low number of complete annual records on streamflow and sediment discharge, and the absence of sub-daily or depth-integrated measurements of sediment concentrations, we regard the decadal sediment data as a conservative estimate for recent catchment erosion. This was also reported for suspended sediments from other rivers of the western Andes (Vanacker et al., 2020; Carretier et al., 2018). In addition, suspended sediments do not record the effects of chemical weathering on denudation rates. This process seems to be relevant in the CCR: in the absence of spatially resolved data of regolith thickness, single observations suggest thick saprolite layers (at least) locally (Vázquez et al., 2016; Mohr et al., 2012; Krone et al., 2021). Thus, depending on the magnitude of mass loss due to chemical weathering, which ranges between 0 and ~240 $T/km^2/a$ in other latitudes of the CCR (Schaller and Ehlers, 2022), total denudation in the short term can be equal or even higher than the long term denudation. Yet, we do not have quantitative estimates of local chemical weathering and soil production rates to test that hypothesis.

The Purapel river catchment has been a staging ground for rapid expansion of tree plantations and a number of disturbances during the period of suspended sediment monitoring. This landscape was affected

by clear-cuts, two widespread wildfires and one Mw 8.8 earthquake. The expansion of tree plantations was mostly at the expense of poorly vegetated surfaces (Fig. 6). Yet, their management includes extensive logging operations – mostly during wet seasons (Fig. 8) – and the construction and maintaining of forestry roads used by heavy machinery. The distribution and density of a road network by itself means an increase in structural sediment connectivity (Fig. 7). Higher connectivity facilitates the routing of detached soils, even from hilltops, where soil production rate is slower compared to the mid-slope or toe positions across the CCR (Schaller and Ehlers, 2022). Thus, hilltop soils may be more difficult to recover during human time scales. The increase in sediment connectivity is distributed along all the hillslopes and more than the half of the catchment experienced at least 2 disturbance events between 2002 and 2019. Despite the disturbances, mean and high (p95) annual values of suspended sediment discharge (Fig. 5) and mean suspended sediment concentrations during the wet seasons (Fig. 4) decreased and remained low after the 2017 fire. In contrast, only the lower percentiles of suspended sediment discharge increased after 2017 wildfire. Such behavior corresponds to baseflow conditions. Regardless, we emphasize that the connectivity index here may be a minimum estimate as we used a coarser digital terrain model compared to the original study.

If the suspended sediment record is representative of the sediment yields on Purapel river, the disturbance regime contrasts with expected responses in sediment mobilization, given observations reported in other landscapes (e.g., Reneau et al., 2007; Brown and Krygier, 1971). Nevertheless, the low values of the AI, i.e. the ratio between annual precipitation and evapotranspiration, indicate increasingly scarce water. A decrease can be also interpreted for the streamflow and the baseflow of the wet seasons, mostly in the Autumn. The sediment detachment and transport may coincide with these negative trends. Sediment mobilization both on hillslopes and streams depends mostly on specific thresholds of rainfall intensity and water discharge, while the unprecedented drought starting in 2010, together with high root water uptake by fast-growing tree plantations resulted in a reduction in water availability. In this scenario, a lack of minimum rainfall intensity required to trigger runoff and soil erosion on hillslopes (Mohr et al., 2013) and/or an increase in the residence time of sediments stored within the valleys is plausible. As rainfall and direct runoff control sediment fluxes at the catchment scale (Andermann et al., 2012; Tolorza et al., 2014), sediment mobilization under the current hydrological regime may stay low despite landscape disturbances. In fact, after the severe and extended 2017 fire (Fig. 6) and after the M_w 8.8 Maule earthquake (Tolorza et al., 2019), sediment discharge remained low at Purapel river. A recent model in post-fire sediment cascades indicates that, even when post-fire erosion may be severe in source areas, a substantial fraction of the detached sediment load may (intermittently) remain stored within valleys with only moderate delivery to the river network (Murphy et al., 2019). Assuming transport limitation under the current drought conditions, prolonged residence times of sediments may be also expected. Indeed, both tree plantations and the drought reduced the recharge of deep soil water reservoirs (Iroumé et al., 2021; Huber et al., 2010). Also the loss of soils due to erosion may further reduce the water-storage capacity (Ratta and Lal, 1998). The long deficit of water due to the drought and the tree plantations may reduce groundwater storage, which is consistent with the observed negative trend in baseflow. Such sharp reduction in water availability may limit the sediment transport in channels. The increase of the sediment transport only for the lower percentiles supports the notion that sediment transport is largely restricted to baseflow conditions during the study period. Hence, we cannot unambigously quantify the overall effect of landscape disturbances on sediment fluxes. Sediment fluxes are more efficient during periods of high flows which correspond to wetter conditions (e.g., Mohr et al., 2013). Consequently, the sediment stored in the valleys, highly rich in nutrients and carbon, can be re-suspended

during higher discharge events, causing temporarily delayed off-site problems for several decades to come.

The expansion of tree plantations has been proposed as a tool to mitigate soil erosion (CONAF and MINAGRI, 2016). Recently, plantations have been favored as a better solution to mitigate soil erosion compared to native forests for the same Purapel catchment (Pizarro et al., 2020). A direct comparison between native forest and plantations cannot be done for the period 1986-2018, because the major land cover transition was from poorly vegetated surfaces to tree plantations (Fig. 6). Nevertheless, we can discuss whether the observed land management is a suitable solution for soil erosion mitigation in the CCR. There is abundant evidence of increased soil erosion in Chilean tree plantations, such as truncated soil profiles in an eucalyptus stand at 36º37'S (Banfield et al., 2018), a fourfold increase in net soil loss under pine stands relative to native forest at Talcamavida (37º7'S) and Nacimiento (37º30'S) (Aburto et al., 2020) or changes in nutrient cycles and increased sedimentation rates in coastal lakes, such as Matanza (33º45'S, Fuentealba et al., 2020), Vichuquén (34ºS, Fuentealba et al., 2021), San Pedro (36º51', Cisternas et al., 2001), and Lanalhue (37ºS, Alaniz et al., 2021). Based on such strong empirical evidence along CCR and our own results (Fig. 2, 6, 7 and 8), we argue that the observed ongoing forest management of tree plantations promotes soil erosion and landscape degradation. In addition, soils in tree plantations are depleted in carbon and nutrients (Soto et al., 2019; Banfield et al., 2018), and inhibit lower invertebrate diversity (Cifuentes-Croquevielle et al., 2020) compared to soils under native forest. As a result, C and N stocks are relatively lower in tree plantations up to deep soil compartments (>120 cm) (Crovo et al., 2021). Soil organic matter is a key component for soil formation (Bernhard et al., 2018). For that reason alone, native forests rather than exotic tree plantations are a more appropriate land cover to regenerate soils and reverse or, at least, decelerate 200 years of intense soil erosion. Indeed, the protection and conservation of natural vegetation has the strongest effect on soil quality after water erosion (Vanacker et al., 2022), and the few empirical restoration examples of native forest in former Eucalyptus plantations has promising increases for water availability (Lara et al., 2021).

Conclusion

The Purapel catchment, as other similar catchments along the CCR, denudates slowly on scales of 10^3 to 10^4 years. The averaged suspended sediment discharge is similar in magnitude, although likely underestimating total denudation. Then, depending on the magnitude of the unmeasured portion of the denudation, decadal lowering of Earth Surface may be equal or even higher that the long-term average.

Suspended sediment transport decreases during the wet seasons between 1986 and 2018, which, at first glance, conflicts with the disturbances observed in vegetation, especially the intense and widespread wild-fires. The decrease in several hydroclimatic measures, including baseflow and aridity, coincides with lower suspended sediment loads. We argue that the low range of recent suspended sediment discharge resulted from limitations in the detachment and transport of sediments due to the overall observed water scarcity. Or in other words: The drought offsets the effects of the disturbances and the higher connectivity. Without sufficient water, residence times of sediments are long, despite the increased sediment connectivity on hillslopes. The contribution of tree plantations to reduce erosion, if any, seems to be more related to their impact in water availability than directly in soil protection.

Because the surface lowering in the last 3 decades is similar to or higher than the long-term benchmark and those measures are spread along a specific dry period, we argue it may be considered high for this specific

system. That conclusion and the documented effects of tree plantations on SOC and soil biodiversity are indicators of a degrading landscape.

References

F. Aburto, E. Cartes, O. Mardones, and R. Rubilar. Hillslope soil erosion and mobility in exotic pine plantations and native deciduous forest in the coastal range of south-central Chile. *Land Degradation & Development*, page ldr.3700, 6 2020. ISSN 1085-3278. doi: 10.1002/ldr.3700. URL `https://onlinelibrary.wiley.com/doi/abs/10.1002/ldr.3700`.

A. J. Alaniz, A. M. Abarzúa, A. Martel-Cea, L. Jarpa, M. Hernández, M. A. Aquino-López, and C. Smith-Ramírez. Linking sedimentological and spatial analysis to assess the impact of the forestry industry on soil loss: The case of Lanalhue Basin, Chile. *Catena*, 207, 12 2021. ISSN 03418162. doi: 10.1016/j.catena.2021.105660.

C. Álvarez-Garreton, P. A. Mendoza, J. P. Boisier, N. Addor, M. Galleguillos, M. Zambrano-Bigiarini, A. Lara, C. Puelma, G. Cortes, R. Garreaud, J. McPhee, and A. Ayala. The CAMELS-CL dataset: catchment attributes and meteorology for large sample studies – Chile dataset. *Hydrology and Earth System Sciences Discussions*, pages 1–40, 2 2018. ISSN 1812-2116. doi: 10.5194/hess-2018-23. URL `https://www.hydrol-earth-syst-sci-discuss.net/hess-2018-23/`.

C. Andermann, A. Crave, R. Gloaguen, P. Davy, and S. Bonnet. Connecting source and transport: Suspended sediments in the Nepal Himalayas. *Earth and Planetary Science Letters*, 351-352:158–170, 2012. ISSN 0012821X. doi: 10.1016/j.epsl.2012.06.059. URL `http://dx.doi.org/10.1016/j.epsl.2012.06.059`.

J. J. Armesto, D. Manuschevich, A. Mora, C. Smith-Ramirez, R. Rozzi, A. M. Abarzúa, and P. a. Marquet. From the Holocene to the Anthropocene: A historical framework for land cover change in southwestern South America in the past 15,000 years. *Land Use Policy*, 27(2):148–160, 2010. ISSN 02648377. doi: 10.1016/j.landusepol.2009.07.006. URL `http://dx.doi.org/10.1016/j.landusepol.2009.07.006`.

C. C. Banfield, A. C. Braun, R. Barra, A. Castillo, and J. Vogt. Erosion proxies in an exotic tree plantation question the appropriate land use in Central Chile. *CATENA*, 161:77–84, 2 2018. ISSN 03418162. doi: 10.1016/j.catena.2017.10.017. URL `http://linkinghub.elsevier.com/retrieve/pii/S0341816217303399`.

S. Barros. Evolución de las plantaciones forestales en Chile. Forestación y reforestación. *Ciencia e Investigación Forestal*, 24(3):89–115, 2018. URL `https://bibliotecadigital.infor.cl/handle/20.500.12220/28235`.

N. Bernhard, L.-M. Moskwa, K. Schmidt, R. A. Oeser, F. Aburto, M. Y. Bader, K. Baumann, F. von Blanckenburg, J. Boy, L. van den Brink, E. Brucker, B. Büdel, R. Canessa, M. A. Dippold, T. A. Ehlers, J. P. Fuentes, R. Godoy, P. Jung, U. Karsten, M. Köster, Y. Kuzyakov, P. Leinweber, H. Neidhardt, F. Matus, C. W. Mueller, Y. Oelmann, R. Oses, P. Osses, L. Paulino, E. Samolov, M. Schaller, M. Schmid, S. Spielvogel, M. Spohn, S. Stock, N. Stroncik, K. Tielbörger, K. Übernickel, T. Scholten, O. Seguel, D. Wagner, and P. Kühn. Pedogenic and microbial interrelations to regional climate and

local topography: New insights from a climate gradient (arid to humid) along the Coastal Cordillera of Chile. *CATENA*, 170:335–355, 11 2018. ISSN 03418162. doi: 10.1016/j.catena.2018.06.018. URL https://doi.org/10.1016/j.catena.2018.06.018https://linkinghub.elsevier.com/retrieve/pii/S0341816218302509https://www.researchgate.net/publication/268272012_Tools_to_aid_post-wildfire_assessment_and_erosion-mitigation_treatment_decisions.

V. Bianchi-Gundian. *Erosión. Cáncer del suelo.* Imprenta Universitaria, Santiago de Chile, 1947.

K. D. Bladon, M. B. Emelko, U. Silins, and M. Stone. Wildfire and the Future of Water Supply. *Environmental Science & Technology*, 48(16):8936–8943, 8 2014. ISSN 0013-936X. doi: 10.1021/es500130g. URL https://pubs.acs.org/doi/10.1021/es500130g.

J. Boardman, K. Vandaele, R. Evans, and I. D. Foster. Off-site impacts of soil erosion and runoff: Why connectivity is more important than erosion rates. *Soil Use and Management*, 35(2):245–256, 6 2019. ISSN 14752743. doi: 10.1111/sum.12496.

J. P. Boisier, C. Alvarez-Garretón, J. Cepeda, A. Osses, N. Vásquez, and R. Rondanelli. CR2MET: A high-resolution precipitation and temperature dataset for hydroclimatic research in Chile. In *EGU General Assembly Conference Abstracts*, EGU General Assembly Conference Abstracts, page 19739, 4 2018a. URL https://meetingorganizer.copernicus.org/EGU2018/EGU2018-19739.pdf.

J. P. Boisier, C. Alvarez-Garreton, R. R. Cordero, A. Damiani, L. Gallardo, R. D. Garreaud, F. Lambert, C. Ramallo, M. Rojas, and R. Rondanelli. Anthropogenic drying in central-southern Chile evidenced by long-term observations and climate model simulations. *Elementa*, 6, 2018b. ISSN 23251026. doi: 10.1525/elementa.328.

C. A. Bonilla and O. I. Johnson. Soil erodibility mapping and its correlation with soil properties in Central Chile. *Geoderma*, 189-190:116–123, 11 2012. ISSN 00167061. doi: 10.1016/j.geoderma.2012.05.005. URL https://linkinghub.elsevier.com/retrieve/pii/S0016706112001966.

P. Borrelli, D. A. Robinson, P. Panagos, E. Lugato, J. E. Yang, C. Alewell, D. Wuepper, L. Montanarella, and C. Ballabio. Land use and climate change impacts on global soil erosion by water (2015-2070). *Proceedings of the National Academy of Sciences of the United States of America*, 117(36):21994–22001, 2020. ISSN 10916490. doi: 10.1073/pnas.2001403117.

D. M. J. S. Bowman, A. Moreira-Muñoz, C. A. Kolden, R. O. Chávez, A. A. Muñoz, F. Salinas, A. González-Reyes, R. Rocco, F. de la Barrera, G. J. Williamson, N. Borchers, L. A. Cifuentes, J. T. Abatzoglou, and F. H. Johnston. Human–environmental drivers and impacts of the globally extreme 2017 Chilean fires. *Ambio*, 48(4):350–362, 4 2019. ISSN 0044-7447. doi: 10.1007/s13280-018-1084-1.

G. W. Brown and J. T. Krygier. Clear-Cut Logging and Sediment Production in the Oregon Coast Range. *Water Resources Research*, 7(5):1189–1198, 1971. ISSN 19447973. doi: 10.1029/WR007i005p01189.

J. Cabezas and F. E. Fassnacht. Reconstructing the Vegetation Disturbance History of a Biodiversity Hotspot in Central Chile Using Landsat, Bfast and Landtrendr. In *IGARSS 2018 - 2018 IEEE International Geoscience and Remote Sensing Symposium*, pages 7636–7639. IEEE, 7 2018. ISBN 978-1-5386-7150-4. doi: 10.1109/IGARSS.2018.8518863.

S. Carretier, V. Tolorza, V. Regard, G. Aguilar, M. Bermúdez, J. Martinod, J.-L. Guyot, G. Hérail, and R. Riquelme. Review of erosion dynamics along the major N-S climatic gradient in Chile and perspectives. *Geomorphology*, 300:45–68, 1 2018. ISSN 0169555X. doi: 10.1016/j.geomorph.2017.10.016. URL `https://www.sciencedirect.com/science/article/pii/S0169555X17304506https://linkinghub.elsevier.com/retrieve/pii/S0169555X17304506`.

M. Cavalli, S. Trevisani, F. Comiti, and L. Marchi. Geomorphometric assessment of spatial sediment connectivity in small Alpine catchments. *Geomorphology*, 188:31–41, 2013. ISSN 0169555X. doi: 10.1016/j.geomorph.2012.05.007. URL `http://dx.doi.org/10.1016/j.geomorph.2012.05.007`.

Chilean Law 19.300. Decreto 40. Reglamento del Sistema de Evaluación de Impacto Ambiental, 2013. URL `http://bcn.cl/2f8a8`.

E. Chuvieco. *Teledeteccion Ambiental: la observacion de la tierra desde el espacio. 3a edicion.* Ariel Ciencia, Barcelona, 2008. ISBN 978-84-344-8072-8.

C. Cifuentes-Croquevielle, D. E. Stanton, and J. J. Armesto. Soil invertebrate diversity loss and functional changes in temperate forest soils replaced by exotic pine plantations. *Scientific Reports*, 10(1): 7762, 12 2020. ISSN 2045-2322. doi: 10.1038/s41598-020-64453-y. URL `http://dx.doi.org/10.1038/s41598-020-64453-yhttp://www.nature.com/articles/s41598-020-64453-y`.

CIREN. Cuenca Río Purapel (Estados erosivos actuales), 2021. URL `http://erosionmaule.ciren.cl/documents/348`.

M. Cisternas, A. Araneda, P. Martinez, and S. Perez. Effects of historical land use on sediment yield from a lacustrine watershed in central Chile. *Earth Surface Processes and Landforms*, 26(1):63–76, 1 2001. ISSN 0197-9337. doi: 10.1002/1096-9837(200101)26:1⟨63::AID-ESP157⟩3.0.CO;2-J. URL `https://onlinelibrary.wiley.com/doi/10.1002/1096-9837(200101)26:1<63::AID-ESP157>3.0.CO;2-J`.

W. S. Cleveland. LOWESS: A Program for Smoothing Scatterplots by Robust Locally Weighted Regression. *The American Statistician*, 35(1):54, 2 1981. ISSN 00031305. doi: 10.2307/2683591. URL `https://www.jstor.org/stable/2683591?origin=crossref`.

CONAF and MINAGRI. Decreto Ley 701 de 1974, Cuarenta años de incentivos a la forestación (1975-2015), 2016. URL `https://biblioteca.digital.gob.cl/handle/123456789/2334`.

L. Cortés, H. J. Hernández, and P. Silva. Historic Land Cover Change assesment of Chilean Mediterranean Coast: Did forest plantations really caused fragmentation? *ISPRS Annals of the Photogrammetry, Remote Sensing and Spatial Information Sciences*, V-3-2022:383–388, 5 2022. ISSN 2194-9050. doi: 10.5194/isprs-annals-V-3-2022-383-2022. URL `https://www.isprs-ann-photogramm-remote-sens-spatial-inf-sci.net/V-3-2022/383/2022/`.

J. A. Covault, W. H. Craddock, B. W. Romans, A. Fildani, and M. Gosai. Spatial and Temporal Variations in Landscape Evolution: Historic and Longer-Term Sediment Flux through Global Catchments. *The Journal of Geology*, 121(1):35–56, 1 2013. ISSN 00221376. doi: 10.1086/668680. URL `http://www.jstor.org/stable/info/10.1086/668680`.

O. Crovo, F. Aburto, M. F. Albornoz, and R. Southard. Soil type modulates the response of C, N, P stocks and stoichiometry after native forest substitution by exotic plantations. *CATENA*, 197:104997, 2 2021. ISSN 03418162. doi: 10.1016/j.catena.2020.104997. URL https://linkinghub.elsevier.com/retrieve/pii/S0341816220305476.

D. A. DellaSala. "Real" vs. "Fake" Forests: Why Tree Plantations Are Not Forests. In *Encyclopedia of the World's Biomes*, volume 3-5, pages 47–55. Elsevier, 6 2020. ISBN 9780128160978. doi: 10.1016/B978-0-12-409548-9.11684-7. URL https://linkinghub.elsevier.com/retrieve/pii/B9780124095489116847.

E. C. Ellis and N. Ramankutty. Putting people in the map: anthropogenic biomes of the world. *Frontiers in Ecology and the Environment*, 6(8):439–447, 10 2008. ISSN 1540-9295. doi: 10.1890/070062. URL http://doi.wiley.com/10.1890/070062.

S. Foga, P. L. Scaramuzza, S. Guo, Z. Zhu, R. D. Dilley, T. Beckmann, G. L. Schmidt, J. L. Dwyer, M. Joseph Hughes, and B. Laue. Cloud detection algorithm comparison and validation for operational Landsat data products. *Remote Sensing of Environment*, 194:379–390, 6 2017. ISSN 00344257. doi: 10.1016/j.rse.2017.03.026.

M. Fuentealba, C. Latorre, M. Frugone-Álvarez, P. Sarricolea, S. Giralt, M. Contreras-Lopez, R. Prego, P. Bernárdez, and B. Valero-Garcés. A combined approach to establishing the timing and magnitude of anthropogenic nutrient alteration in a mediterranean coastal lake- watershed system. *Scientific Reports*, 10(1):5864, 12 2020. ISSN 2045-2322. doi: 10.1038/s41598-020-62627-2. URL http://www.nature.com/articles/s41598-020-62627-2.

M. Fuentealba, C. Latorre, M. Frugone-Álvarez, P. Sarricolea, C. Godoy-Aguirre, J. Armesto, L. A. Villacís, M. Laura Carrevedo, O. Meseguer-Ruiz, and B. Valero-Garcés. Crossing a critical threshold: Accelerated and widespread land use changes drive recent carbon and nitrogen dynamics in Vichuquén Lake (35°S) in central Chile. *Science of the Total Environment*, 791, 10 2021. ISSN 18791026. doi: 10.1016/j.scitotenv.2021.148209.

E. J. Gabet, S. M. Mudd, R. W. Wood, S. W. D. Grieve, S. A. Binnie, and T. J. Dunai. Hilltop Curvature Increases With the Square Root of Erosion Rate. *Journal of Geophysical Research: Earth Surface*, 126(5):1–16, 2021. ISSN 2169-9003. doi: 10.1029/2020jf005858.

M. Galleguillos, F. Gimeno, C. Puelma, M. Zambrano-Bigiarini, A. Lara, and M. Rojas. Disentangling the effect of future land use strategies and climate change on streamflow in a Mediterranean catchment dominated by tree plantations. *Journal of Hydrology*, 595(February), 2021. ISSN 00221694. doi: 10.1016/j.jhydrol.2021.126047.

R. D. Garreaud, J. P. Boisier, R. Rondanelli, A. Montecinos, H. H. Sepúlveda, and D. Veloso-Aguila. The Central Chile Mega Drought (2010–2018): A climate dynamics perspective. *International Journal of Climatology*, 40(1):421–439, 1 2020. ISSN 0899-8418. doi: 10.1002/joc.6219. URL https://onlinelibrary.wiley.com/doi/10.1002/joc.6219.

V. Gerding. Manejo de las plantaciones de Pinus radiata D. Don en Chile. *Bosque*, 12(2):3–10, 1991.

F. Gimeno, M. Galleguillos, D. Manuschevich, and M. Zambrano-Bigiarini. A coupled modeling approach to assess the effect of forest policies in water provision: A biophysical evaluation of a drought-prone rural catchment in south-central Chile. *Science of The Total Environment*, 830:154608, 7 2022. ISSN 00489697. doi: 10.1016/j.scitotenv.2022.154608.

S. Gómez-González, S. Paula, L. A. Cavieres, and J. G. Pausas. Postfire responses of the woody flora of Central Chile: Insights from a germination experiment. *PLoS ONE*, 12(7):1–12, 2017. ISSN 19326203. doi: 10.1371/journal.pone.0180661.

S. Gómez-González, F. Ojeda, and P. M. Fernandes. Portugal and Chile: Longing for sustainable forestry while rising from the ashes. *Environmental Science & Policy*, 81:104–107, 3 2018. ISSN 14629011. doi: 10.1016/j.envsci.2017.11.006. URL https://linkinghub.elsevier.com/retrieve/pii/S1462901117307694.

D. E. Granger and M. Schaller. Cosmogenic Nuclides and Erosion at the Watershed Scale. *Elements*, 10(5):369–373, 10 2014. ISSN 1811-5209. doi: 10.2113/gselements.10.5.369. URL https://pubs.geoscienceworld.org/elements/article/10/5/369-373/137626.

M. C. Hansen, P. V. Potapov, R. Moore, M. Hancher, S. A. Turubanova, A. Tyukavina, D. Thau, S. V. Stehman, S. J. Goetz, T. R. Loveland, A. Kommareddy, A. Egorov, L. Chini, C. O. Justice, and J. R. G. Townshend. High-Resolution Global Maps of 21st-Century Forest Cover Change. *Science*, 342(6160): 850–853, 11 2013. ISSN 0036-8075. doi: 10.1126/science.1244693. URL http://www.sciencemag.org/cgi/doi/10.1126/science.1244693.

R. Heilmayr, C. Echeverría, R. Fuentes, and E. F. Lambin. A plantation-dominated forest transition in Chile. *Applied Geography*, 75:71–82, 2016. ISSN 01436228. doi: 10.1016/j.apgeog.2016.07.014. URL http://dx.doi.org/10.1016/j.apgeog.2016.07.014.

D. R. Helsel, R. M. Hirsch, K. R. Ryberg, S. A. Archfield, and E. J. Gilroy. Statistical methods in water resources. Technical report, USGS, Reston, VA, 2020. URL http://pubs.er.usgs.gov/publication/tm4A3.

K. Hermosilla-Palma, P. Pliscoff, and M. Folchi. Sixty years of land-use and land-cover change dynamics in a global biodiversity hotspot under threat from global change. *Journal of Land Use Science*, 16(5-6):467–478, 11 2021. ISSN 1747-423X. doi: 10.1080/1747423X.2021.2011970. URL https://www.tandfonline.com/doi/full/10.1080/1747423X.2021.2011970.

T. Hewawasam, F. von Blanckenburg, M. Schaller, and P. Kubik. Increase of human over natural erosion rates in tropical highlands constrained by cosmogenic nuclides. *Geology*, 31(7):597–600, 2003. ISSN 00917613. doi: 10.1130/0091-7613(2003)031⟨0597:IOHONE⟩2.0.CO;2. URL http://geology.gsapubs.org/content/31/7/597.abstract.

S. Huang, Q. Dong, X. Zhang, and W. Deng. Catchment natural driving factors and prediction of baseflow index for Continental United States based on Random Forest technique. *Stochastic Environmental Research and Risk Assessment*, 35(12):2567–2581, 12 2021. ISSN 14363259. doi: 10.1007/s00477-021-02057-2.

A. Huber, A. Iroumé, C. Mohr, and C. Frêne. Effect of Pinus radiata and Eucalyptus globulus plantations on water resource in the Coastal Range of Biobio region, Chile. *Bosque (Valdivia)*, 31(3):219–230, 2010. ISSN 0717-9200. doi: 10.4067/S0717-92002010000300006. URL `http://www.scielo.cl/scielo.php?script=sci_arttext&pid=S0717-92002010000300006&lng=en&nrm=iso&tlng=en`.

F. Imaizumi, R. C. Sidle, and R. Kamei. Effects of forest harvesting on the occurrence of landslides and debris flows in steep terrain of central Japan. *Earth Surface Processes and Landforms*, 33(6):827–840, 5 2008. ISSN 01979337. doi: 10.1002/esp.1574. URL `http://www3.interscience.wiley.com/journal/121517813/abstracthttp://doi.wiley.com/10.1002/esp.1574`.

INFOR. Informe Técnico 165: Eucalyptus nitens en Chile: primera monografía. Technical report, INFOR, Valdivia, 2004. URL `https://bibliotecadigital.infor.cl/handle/20.500.12220/7741?show=full`.

IPCC. Regional Fact Sheet – Central and South America in: Sixth Assessment Report. Working Group I – The Physical Science Basis. *Ipcc*, page 2, 2021. URL `https://www.ipcc.ch/assessment-report/ar6/`.

IREN. Evaluación de la erosión Cordillera de la Costa entre Valparaíso y Cautín. Technical report, Instituto de Investigación de Recursos Naturales, Instituto de Investigación de Recursos Naturales, Santiago, Chile, 1965. URL `http://bibliotecadigital.ciren.cl/handle/123456789/14283`.

A. Iroumé, O. Mayen, and A. Huber. Runoff and peak flow responses to timber harvest and forest age in southern Chile. *Hydrological Processes*, 20(1):37–50, 2006. ISSN 08856087. doi: 10.1002/hyp.5897.

A. Iroumé, J. Jones, and J. C. Bathurst. Forest operations, tree species composition and decline in rainfall explain runoff changes in the Nacimiento experimental catchments, south central Chile. *Hydrological Processes*, 35(6):1–21, 2021. ISSN 0885-6087. doi: 10.1002/hyp.14257.

C. H. Key and N. C. Benson. Landscape Assessment (LA) sampling and analysis methods. In *Lutes, Duncan C.; Keane, Robert E.; Caratti, John F.; Key, Carl H.; Benson, Nathan C.; Sutherland, Steve; Gangi, Larry J. FIREMON: Fire effects monitoring and inventory system. Gen. Tech. Rep. RMRS-GTR-164-CD*, pages LA1–LA51. US Department of Agriculture, Forest Service, Rocky Mountain Research Station, 2006. URL `https://www.fs.usda.gov/treesearch/pubs/24066`.

J. W. Kirchner, R. C. Finkel, C. S. Riebe, D. E. Granger, J. L. Clayton, J. G. King, and W. F. Megahan. Mountain erosion over 10 yr, 10 k.y., and 10 m.y. time scales. *Geology*, 29(7):591, 2001. ISSN 0091-7613. doi: 10.1130/0091-7613(2001)029⟨0591:MEOYKY⟩2.0.CO;2. URL `http://geology.gsapubs.org/content/29/7/591.abstracthttps://pubs.geoscienceworld.org/geology/article/29/7/591-594/188782`.

L. V. Krone, F. J. Hampl, C. Schwerdhelm, C. Bryce, L. Ganzert, A. Kitte, K. Übernickel, A. Dielforder, S. Aldaz, R. Oses-Pedraza, J. P. H. Perez, P. Sanchez-Alfaro, D. Wagner, U. Weckmann, and F. von Blanckenburg. Deep weathering in the semi-arid Coastal Cordillera, Chile. *Scientific Reports*, 11(1), 12 2021. ISSN 20452322. doi: 10.1038/s41598-021-90267-7.

A. Ladson, R. Brown, B. Neal, and R. Nathan. A standard approach to baseflow separation using the Lyne and Hollick filter. *Australian Journal of Water Resources*, 17(1), 2013. ISSN 13241583. doi: 10.7158/W12-028.2013.17.1. URL `http://www.engineersmedia.com.au/journals/ajwr/2013/17_1/W12_028.html`.

D. Lal. Cosmic ray labeling of erosion surfaces: in situ nuclide production rates and erosion models. *Earth and Planetary Science Letters*, 104(2-4):424–439, 6 1991. ISSN 0012821X. doi: 10.1016/0012-821X(91)90220-C. URL https://linkinghub.elsevier.com/retrieve/pii/0012821X9190220C.

A. Lara, J. Jones, C. Little, and N. Vergara. Streamflow response to native forest restoration in former Eucalyptus plantations in south central Chile. *Hydrological Processes*, 35(8), 8 2021. ISSN 10991085. doi: 10.1002/hyp.14270.

M. Li, S. Li, Q. Liu, Y. Kang, L. Liang, X. Yuan, J. Zhang, X. Wang, and C. Li. Assessment of hydrological response to multiyear drought: Insights from lag characteristics and shift magnitude. *Hydrological Processes*, 36(7), 7 2022. ISSN 10991085. doi: 10.1002/hyp.14636.

A. Malmer and H. Grip. Soil disturbance and loss of infiltrability caused by mechanized and manual extraction of tropical rainforest in Sabah, Malaysia. *Forest Ecology and Management*, 38(1-2):1–12, 12 1990. ISSN 03781127. doi: 10.1016/0378-1127(90)90081-L. URL http://linkinghub.elsevier.com/retrieve/pii/037811279090081L.

D. Manuschevich. Land use as a socio-ecological system: Developing a transdisciplinary approach to studies of land use change in South-Central Chile. In *Ecological Economic and Socio Ecological Strategies for Forest Conservation: A Transdisciplinary Approach Focused on Chile and Brazil*, pages 79–97. Springer International Publishing, 1 2020. ISBN 9783030353797. doi: 10.1007/978-3-030-35379-7{_}5.

L. Martini, M. Cavalli, and L. Picco. Predicting sediment connectivity in a mountain basin: A quantitative analysis of the index of connectivity. *Earth Surface Processes and Landforms*, 5 2022. ISSN 10969837. doi: 10.1002/esp.5331.

M. A. Martins, A. I. Machado, D. Serpa, S. A. Prats, S. R. Faria, M. E. Varela, O. González-Pelayo, and J. J. Keizer. Runoff and inter-rill erosion in a Maritime Pine and a Eucalypt plantation following wildfire and terracing in north-central Portugal. *Journal of Hydrology and Hydromechanics*, 61(4):261–268, 12 2013. ISSN 0042-790X. doi: 10.2478/johh-2013-0033. URL https://content.sciendo.com/doi/10.2478/johh-2013-0033.

V. Méndez-Freire, T. Villaseñor, and C. Mellado. Spatial and temporal changes in suspended sediment fluxes in central Chile induced by the mega drought: The case of the Itata River Basin (36°-37°S). *Journal of South American Earth Sciences*, 118, 10 2022. ISSN 08959811. doi: 10.1016/j.jsames.2022.103930.

C. Mohr. *Hydrological and erosion responses to man-made and natural disturbances – Insights from forested catchments in South-central Chile*. PhD thesis, University of Potsdam, 2013. URL https://publishup.uni-potsdam.de/opus4-ubp/frontdoor/deliver/index/docId/6782/file/mohr_diss.pdf.

C. H. Mohr, D. R. Montgomery, A. Huber, A. Bronstert, and A. Iroumé. Streamflow response in small upland catchments in the Chilean coastal range to the Mw 8.8 Maule earthquake on 27 February 2010. *Journal of Geophysical Research*, 117(F2):F02032, 6 2012. ISSN 0148-0227. doi: 10.1029/2011JF002138. URL http://doi.wiley.com/10.1029/2011JF002138.

C. H. Mohr, R. Coppus, A. Iroumé, A. Huber, and A. Bronstert. Runoff generation and soil erosion processes after clear cutting. *Journal of Geophysical Research: Earth Surface*, 118(2):814–831, 2013. ISSN 21699003. doi: 10.1002/jgrf.20047. URL http://doi.wiley.com/10.1002/jgrf.20047.

C. H. Mohr, A. Zimmermann, O. Korup, A. Iroumé, T. Francke, and A. Bronstert. Seasonal logging, process response, and geomorphic work. *Earth Surface Dynamics*, 2(1):117–125, 3 2014. ISSN 2196-632X. doi: 10.5194/esurf-2-117-2014. URL `http://www.earth-surf-dynam.net/2/117/2014/`.

D. R. Montgomery, K. M. Schmidt, H. M. Greenberg, and W. E. Dietrich. Forest clearing and regional landsliding. *Geology*, 28(4):311–314, 2000. ISSN 00917613. doi: 10.1130/0091-7613(2000)28⟨311:FCARL⟩ 2.0.CO;2.

J. A. Moody and D. A. Martin. Synthesis of sediment yields after wildland fire in different rainfall regimes in the western United States. *International Journal of Wildland Fire*, 18(1):96, 2009. ISSN 1049-8001. doi: 10.1071/WF07162. URL `http://www.publish.csiro.au/?paper=WF07162`.

B. P. Murphy, J. A. Czuba, and P. Belmont. Post-wildfire sediment cascades: A modeling framework linking debris flow generation and network-scale sediment routing. *Earth Surface Processes and Landforms*, 44 (11):2126–2140, 9 2019. ISSN 0197-9337. doi: 10.1002/esp.4635. URL `https://onlinelibrary.wiley.com/doi/10.1002/esp.4635`.

E. Pepin, S. Carretier, J. L. Guyot, and F. Escobar. Specific suspended sediment yields of the Andean rivers of Chile and their relationship to climate, slope and vegetation. *Hydrological Sciences Journal*, 55(7):1190–1205, 10 2010. ISSN 0262-6667. doi: 10.1080/02626667.2010.512868. URL `http://www.tandfonline.com/doi/abs/10.1080/02626667.2010.512868`.

R. Pizarro, P. García-Chevesich, J. Pino, A. Ibáñez, F. Pérez, J. P. Flores, J. O. Sharp, B. Ingram, R. Mendoza, D. G. Neary, C. Sangüesa, and C. Vallejos. Stabilization of stage–discharge curves following the establishment of forest plantations: Implications for sediment production. *River Research and Applications*, 36(9):1828–1837, 11 2020. ISSN 1535-1459. doi: 10.1002/rra.3718. URL `https://onlinelibrary.wiley.com/doi/10.1002/rra.3718`.

R. Ratta and R. Lal. *Soil quality and soil erosion.* CRC press, 1998. ISBN 1351415735, 9781351415736.

S. L. Reneau, D. Katzman, G. A. Kuyumjian, A. Lavine, and D. V. Malmon. Sediment delivery after a wildfire. *Geology*, 35(2):151–154, 2007. ISSN 00917613. doi: 10.1130/G23288A.1.

J. J. Roering, J. T. Perron, and J. W. Kirchner. Functional relationships between denudation and hillslope form and relief. *Earth and Planetary Science Letters*, 264(1-2):245–258, 2007. ISSN 0012821X. doi: 10.1016/j.epsl.2007.09.035.

M. Schaller and T. A. Ehlers. Comparison of soil production, chemical weathering, and physical erosion rates along a climate and ecological gradient (Chile) to global observations. *Earth Surface Dynamics*, 10(1): 131–150, 2 2022. ISSN 2196-632X. doi: 10.5194/esurf-10-131-2022. URL `https://esurf.copernicus.org/articles/10/131/2022/`.

P. Schuller, D. E. Walling, A. Iroumé, C. Quilodrán, A. Castillo, and A. Navas. Using 137Cs and 210Pbex and other sediment source fingerprints to document suspended sediment sources in small forested catchments in south-central Chile. *Journal of Environmental Radioactivity*, 124:147–159, 2013. ISSN 0265931X. doi: 10.1016/j.jenvrad.2013.05.002. URL `http://dx.doi.org/10.1016/j.jenvrad.2013.05.002`.

P. Schuller, D. E. Walling, A. Iroumé, C. Quilodrán, and A. Castillo. Quantifying the temporal variation of the contribution of fine sediment sources to sediment yields from Chilean forested catchments during harvesting operations. *Bosque (Valdivia)*, 42(2):231–244, 2021. ISSN 0717-9200. doi: 10.4067/S0717-92002021000200231. URL http://www.scielo.cl/scielo.php?script=sci_arttext&pid=S0717-92002021000200231&lng=en&nrm=iso&tlng=en.

A. Serey, L. Piñero-Feliciangeli, S. A. Sepúlveda, F. Poblete, D. N. Petley, and W. Murphy. Landslides induced by the 2010 Chile megathrust earthquake: a comprehensive inventory and correlations with geological and seismic factors. *Landslides*, 3 2019. ISSN 1612-510X. doi: 10.1007/s10346-019-01150-6. URL http://link.springer.com/10.1007/s10346-019-01150-6.

R. C. Sidle and A. D. Ziegler. The dilemma of mountain roads, 7 2012. ISSN 17520894.

W. Solar. Manual de terreno y centros de filtrado. Dirección General de Aguas, 1999. URL https://snia.mop.gob.cl/sad/SED4939.pdf.

L. Soto, M. Galleguillos, O. Seguel, B. Sotomayor, and A. Lara. Assessment of soil physical properties' statuses under different land covers within a landscape dominated by exotic industrial tree plantations in south-central Chile. *Journal of Soil and Water Conservation*, 74(1):12–23, 12 2019. ISSN 0022-4561. doi: 10.2489/jswc.74.1.12. URL http://www.jswconline.org/lookup/doi/10.2489/jswc.74.1.12.

M. a. Summerfield and N. J. Hulton. Natural controls of fluvial denudation rates in major world drainage basins. *Journal of Geophysical Research*, 99(B7):13871–13883, 1994. ISSN 0148-0227. doi: 10.1029/94JB00715. URL http://dx.doi.org/10.1029/94JB00715.

J. Syvitski, J. R. Ángel, Y. Saito, I. Overeem, C. J. Vörösmarty, H. Wang, and D. Olago. Earth's sediment cycle during the Anthropocene. *Nature Reviews Earth & Environment*, 2 2022. ISSN 2662-138X. doi: 10.1038/s43017-021-00253-w. URL https://www.nature.com/articles/s43017-021-00253-w.

C. Teutschbein, T. Grabs, R. H. Karlsen, H. Laudon, and K. Bishop. Hydrological response to changing climate conditions: Spatial streamflow variability in the boreal region. *Water Resources Research*, 51(12):9425–9446, 12 2015. ISSN 19447973. doi: 10.1002/2015WR017337.

V. Tolorza, S. Carretier, C. Andermann, F. Ortega-Culaciati, L. Pinto, and M. Mardones. Contrasting mountain and piedmont dynamics of sediment discharge associated with groundwater storage variation in the Biobío river. *Journal of Geophysical Research: Earth Surface*, 119(12):2730–2753, 2014. ISSN 21699003. doi: 10.1002/2014JF003105. URL http://dx.doi.org/10.1002/2014JF003105http://doi.wiley.com/10.1002/2014JF003105.

V. Tolorza, C. H. Mohr, S. Carretier, A. Serey, S. A. Sepúlveda, J. Tapia, and L. Pinto. Suspended Sediments in Chilean Rivers Reveal Low Postseismic Erosion After the Maule Earthquake (Mw 8.8) During a Severe Drought. *Journal of Geophysical Research: Earth Surface*, m:2018JF004766, 6 2019. ISSN 2169-9003. doi: 10.1029/2018JF004766. URL https://onlinelibrary.wiley.com/doi/abs/10.1029/2018JF004766.

V. Tolorza, D. Poblete-Caballero, D. Banda, C. Little, C. Leal, and M. Galleguillos. An operational method for mapping the composition of post-fire litter. *Remote Sensing Letters*, 13(5):511–521, 5 2022. ISSN

2150-704X. doi: 10.1080/2150704X.2022.2040752. URL `https://www.tandfonline.com/doi/full/10.1080/2150704X.2022.2040752`.

V. Vanacker, F. von Blanckenburg, G. Govers, A. Molina, J. Poesen, J. Deckers, and P. Kubik. Restoring dense vegetation can slow mountain erosion to near natural benchmark levels. *Geology*, 35(4):303, 2007. ISSN 0091-7613. doi: 10.1130/G23109A.1. URL `http://geology.gsapubs.org/cgi/doi/10.1130/G23109A.1`.

V. Vanacker, M. Guns, F. Clapuyt, V. Balthazar, G. Tenorio, and A. Molina. Spatio-temporal patterns of landslides and Erosion in tropical Andean catchments. *Pirineos*, 175, 2020. ISSN 19884281. doi: 10.3989/PIRINEOS.2020.175001.

V. Vanacker, A. Molina, M. Rosas-Barturen, V. Bonnesoeur, F. Román-Dañobeytia, B. F. Ochoa-Tocachi, and W. Buytaert. The effect of natural infrastructure on water erosion mitigation in the Andes. *SOIL*, 8(1):133–147, 2 2022. ISSN 2199-398X. doi: 10.5194/soil-8-133-2022. URL `https://soil.copernicus.org/articles/8/133/2022/`.

M. Vázquez, S. Ramírez, D. Morata, M. Reich, J. J. Braun, and S. Carretier. Regolith production and chemical weathering of granitic rocks in central Chile. *Chemical Geology*, 446:87–98, 2016. ISSN 00092541. doi: 10.1016/j.chemgeo.2016.09.023. URL `http://dx.doi.org/10.1016/j.chemgeo.2016.09.023`.

J. Verbesselt, R. Hyndman, G. Newnham, and D. Culvenor. Detecting trend and seasonal changes in satellite image time series. *Remote Sensing of Environment*, 114(1):106–115, 1 2010. ISSN 00344257. doi: 10.1016/j.rse.2009.08.014. URL `http://linkinghub.elsevier.com/retrieve/pii/S003442570900265X`.

F. von Blanckenburg. The control mechanisms of erosion and weathering at basin scale from cosmogenic nuclides in river sediment. *Earth and Planetary Science Letters*, 237(3-4):462–479, 2005. ISSN 0012821X. doi: 10.1016/j.epsl.2005.06.030. URL `http://www.sciencedirect.com/science/article/pii/S0012821X05004139`.

F. von Blanckenburg and J. K. Willenbring. Cosmogenic Nuclides: Dates and Rates of Earth-Surface Change. *Elements*, 10(5):341–346, 10 2014. ISSN 1811-5209. doi: 10.2113/gselements.10.5.341. URL `http://elements.geoscienceworld.org/content/10/5/341.abstracthttp://elements.geoscienceworld.org/cgi/doi/10.2113/gselements.10.5.341`.

J. Wainwright, L. Turnbull, T. G. Ibrahim, I. Lexartza-Artza, S. F. Thornton, and R. E. Brazier. Linking environmental régimes, space and time: Interpretations of structural and functional connectivity. *Geomorphology*, 126(3-4):387–404, 2011. ISSN 0169555X. doi: 10.1016/j.geomorph.2010.07.027. URL `http://dx.doi.org/10.1016/j.geomorph.2010.07.027`.

E. Wohl, G. Brierley, D. Cadol, T. J. Coulthard, T. Covino, K. A. Fryirs, G. Grant, R. G. Hilton, S. N. Lane, F. J. Magilligan, K. M. Meitzen, P. Passalacqua, R. E. Poeppl, S. L. Rathburn, and L. S. Sklar. Connectivity as an emergent property of geomorphic systems. *Earth Surface Processes and Landforms*, 44(1):4–26, 1 2019. ISSN 01979337. doi: 10.1002/esp.4434. URL `http://doi.wiley.com/10.1002/esp.4434`.

J. Zhang, Y. Zhang, J. Song, and L. Cheng. Evaluating relative merits of four baseflow separation methods in Eastern Australia. *Journal of Hydrology*, 549:252–263, 6 2017. ISSN 00221694. doi: 10.1016/j.jhydrol. 2017.04.004.

Y. Zhao, D. Feng, L. Yu, X. Wang, Y. Chen, Y. Bai, H. J. Hernández, M. Galleguillos, C. Estades, G. S. Biging, J. D. Radke, and P. Gong. Detailed dynamic land cover mapping of Chile: Accuracy improvement by integrating multi-temporal data. *Remote Sensing of Environment*, 183:170–185, 9 2016. ISSN 00344257. doi: 10.1016/j.rse.2016.05.016. URL http://linkinghub.elsevier.com/retrieve/pii/ S0034425716302188.
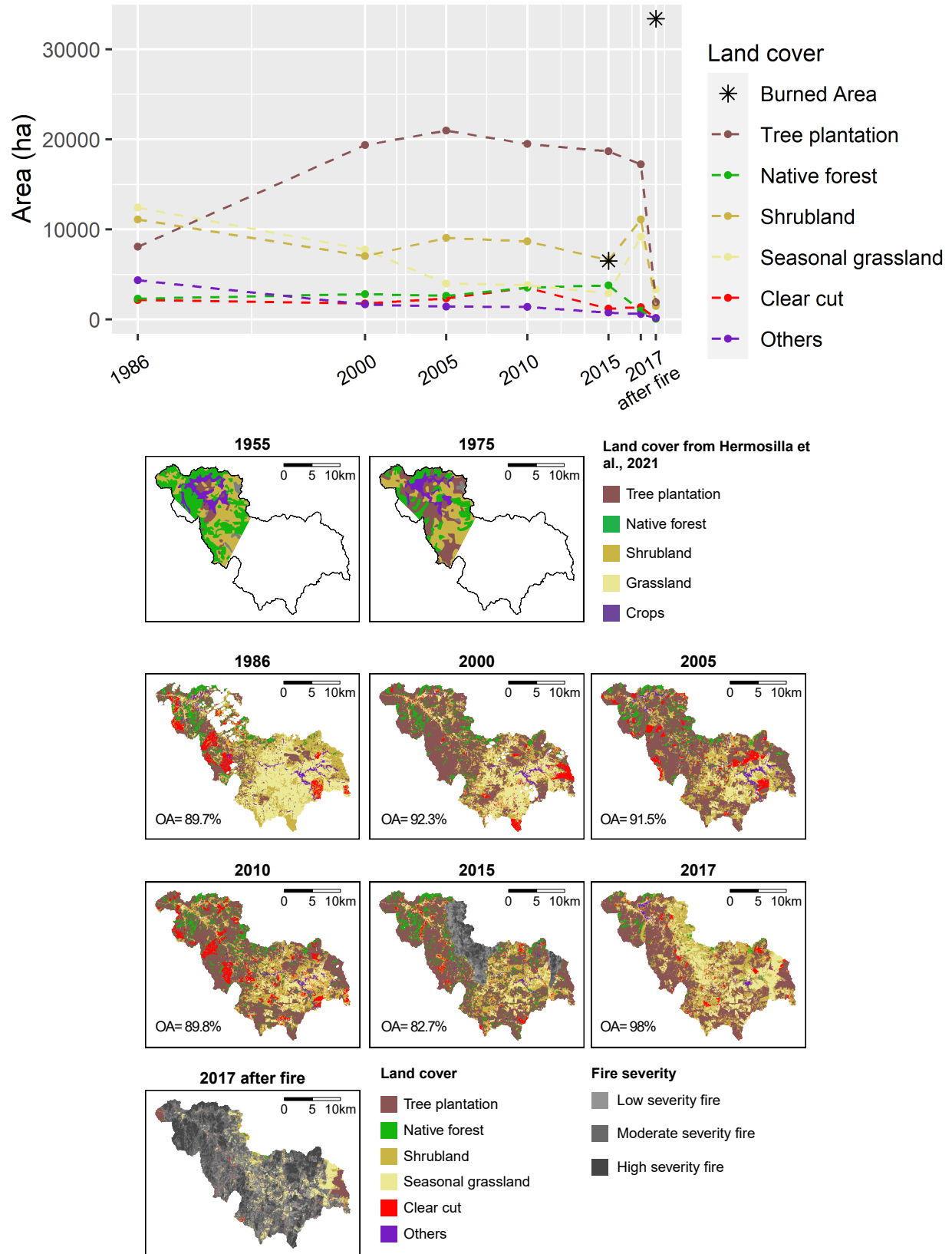
Figure 6: Land cover classification and transitions. Maps of 1955 and 1975 from Hermosilla-Palma et al. (2021), 1986-2015 from this work, and 2017 from Tolorza et al. (2022).
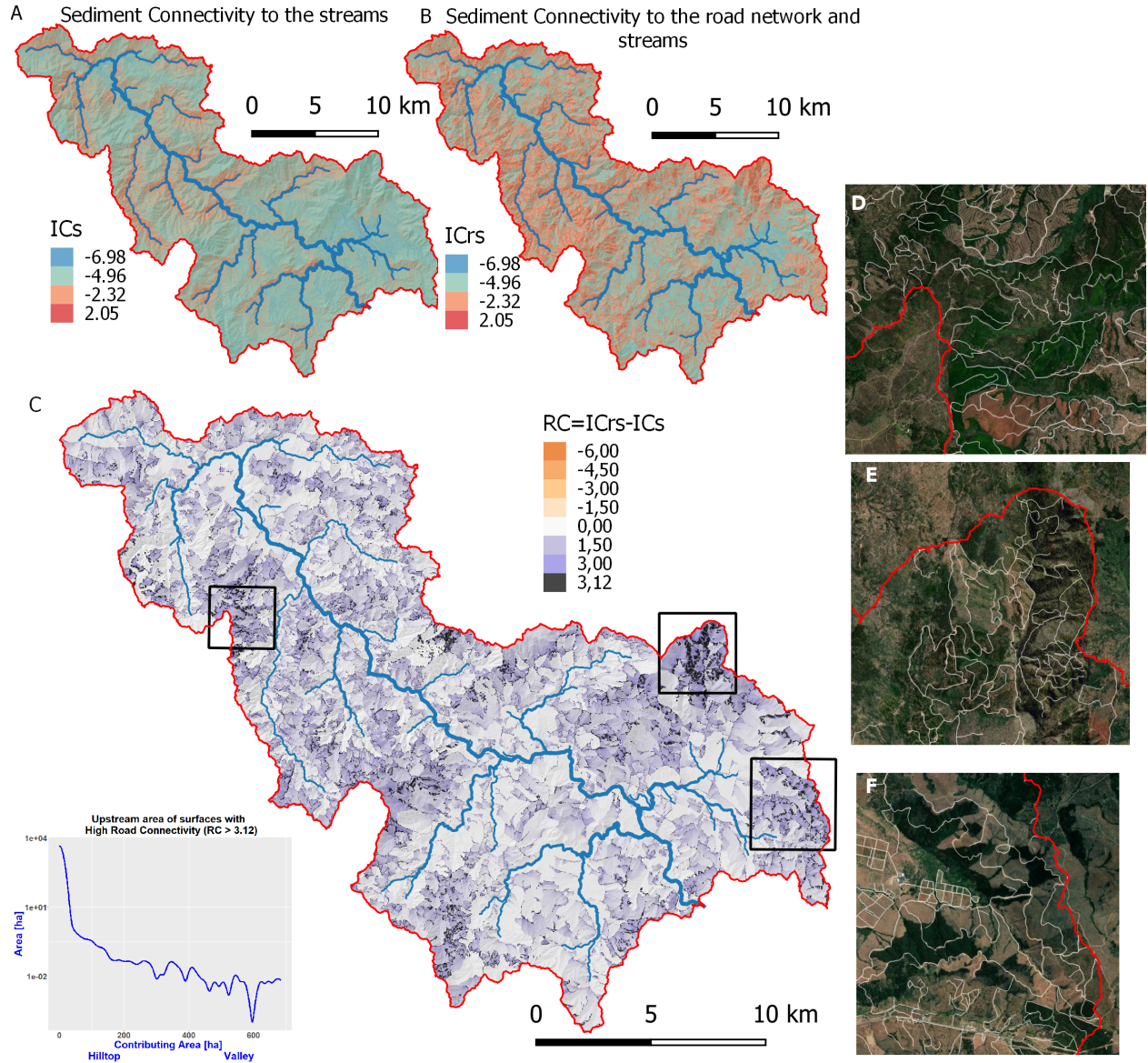
Figure 7: Sediment connectivity index (Cavalli et al., 2013) calculated using (A) the streams and (B) the streams and forest roads as targets. (C) is the difference between both models. (D-F) Details of hilltops with highest values of RC.
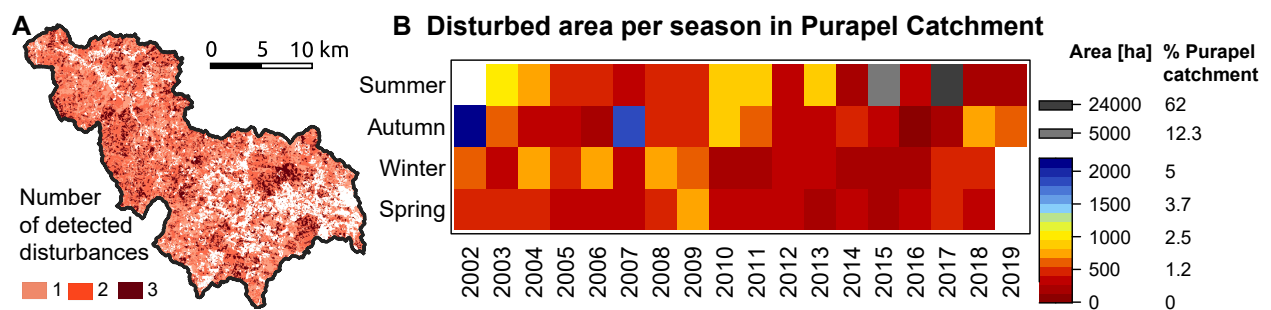
Figure 8: Detected disturbances from BFAST (A) map of the number of disturbances in vegetation detected for the period 2002-2019 (B) Seasonality of disturbance area detected within the Purapel catchment.